This article has been accepted for publication in a future issue of this journal, but has not been fully edited. Content may change prior to final publication. Citation information: DOI 10.1109/TSG.2016.2647620, IEEE Transactions on Smart Grid

Real-Time Smart Charging of Electric Vehicles for Demand Charge Reduction at Non-Residential Sites

Guanchen Zhang, *Student Member, IEEE,* Shaoqing Tim Tan, G. Gary Wang

***Abstract*—Smart Electric Vehicle (EV) charging deals with increasing demand charges caused by EV load on Electric Vehicle Supply Equipment (EVSE) hosts. This paper proposes a real-time smart charging algorithm that can be integrated with Commercial & Industrial (C&I) EVSE hosts through Building Energy Management System (BEMS) or with utility back office through the Advanced Metering Infrastructure (AMI). The proposed charging scheme implements a real-time water-filling algorithm (RTWF-n1) able to reduce the peak demand and to prioritize EV charging based on the data of plugged-in EVs. The algorithm also accommodates utility and local Demand Response and Load Control (DRLC) signals for extensive peak shaving. Real-world EV charging data from different types of venues are used to develop and evaluate the smart charging scheme for demand charge reduction at Medium & Large General Service locations. The results show that even at constrained venues such as large retails, monthly demand charges caused by EVs can be reduced by 20-35% for 30% EV penetration level without depreciating EVs' charging demand.**

***Index Terms*—Electric Vehicle, Smart Charging, Demand Charge, Peak Shaving, Demand Response, Direct Load Control.**

NOMENCLATURE

Abbreviations

AMI	Advanced Metering Infrastructure
BEMS	Building Energy Management System
C&I	Commercial & Industrial
DCFC	DC Fast Charger
DR	Demand Response
DRLC	Demand Response and Load Control
EV	Electric Vehicle
EVSE	EV Supply Equipment
L2	Level-2 Charging (208/240V)
LB	Lower Bound
LGS	Large General Service
MGS	Medium General Service
OPEX	Operational Expense
PHEV	Plug-in Hybrid Electric Vehicle
RTWF	Real-Time Water Filling
SC	Smart Charging
SOC	State of Charge
TOU	Time of Use

Variables

Δt	Smart meter sampling period, or the SC control time step
η	Average charging efficiency
$\mathbf{t_u^*}$	Unplug time of EVs in $\{EV_1\}$ as of t_m
τ_1, τ_2	Start and end time of the DRLC event
θ	Charging flexibility of the $i'th$ EV
$\widetilde{E}$	Average deferrable energy for SC in an EV
$\{EV_1\}$	Group of EVs with the earliest leaving time as of t_m
$\{EV_{(-1)}\}$	Group of EVs not in $\{EV_1\}$ as of t_m
a	Binary term indicating whether the $i'th$ EV is plugged in at time t
E_d	Total energy demand of an EV
$E_d^{'}$	New feasible energy demand after curtailment
$E_{(+)}$	Maximum energy can be charged to $\{EV_{(-1)}\}$ before all EVs in $\{EV_1\}$ leave
$E_{(-)}$	Minimum energy must be charged to $\{EV_{(-1)}\}$ before all EVs in $\{EV_1\}$ leave
$E_\epsilon^{(j)}$	Remaining energy to be charged as of t_m for the $j'th$ EV in $\{EV_1\}$
L_0	Original charging power profile
L_{FD}	Power profile of fully deferrable charging session
L_{PD}	Power profile of partially deferrable charging session
N_t	Number of EVs plugged in at t
N_ν	Number of unplugged EVs (done charging) at $t = t_u$
N_{EV}	Total umber of EVs come to charge in a day
N_{EV}^*	Number of EVs in $\{EV_1\}$
p_c	Constant-current charging power of an EV
p_λ	Provisional lower bound for handling uncertainties towards t_s
P_υ	Upper bound of building-level demand by DRLC at time t
p_υ	Maximum charging power subject to SOC
p_ζ	Applied lower bound for the charging power of the $i'th$ EV at t
p_{min}	Minimum charging power limited by EVSE hardware or software
T	Number of control steps for SC in a day
T_F	Average flexible duration for SC
t_m	Current time in a SC control window
t_p	Plug-in time of an EV
T_s	Number of control steps in each real-time SC window
t_s	End time of a SC control window
t_s^*	Earliest unplug time of EVs in $\{EV_1\}$
t_u	Unplug time of an EV
$x^{(i)}$	Charging power of the $i'th$ EV at $t \in [t_m, t_s]$
x_b	Building's non-EV demand at time t
X_{EV}	Total demand of all plugged-in EVs at time t
Y	Aggregate load profile including building and all EVs
y_t	Total demand in kW at time t

Manuscript submitted on Aug 24, 2016; revised on Nov 29, 2016

The authors are with the School of Mechatronic Systems Engineering, Simon Fraser University, Surrey, B.C., Canada. Emails: gza10@sfu.ca; ttan@sfu.ca; gary_wang@sfu.ca.

This article has been accepted for publication in a future issue of this journal, but has not been fully edited. Content may change prior to final publication. Citation information: DOI 10.1109/TSG.2016.2647620, IEEE Transactions on Smart Grid

I. Introduction

In Canada, EV sales increased by 32% in 2015 [1]. L2 EVSE almost doubled, and the number of DCFCs increased by 250% in 2015 [2]. Large EV charging loads impose new challenges on the power grid in terms of higher peak load and infrastructure overloading. On a smaller scale, excessive EV loading may increase demand charges on EVSE hosts.

EV SC based on various objectives target at different scales and levels. This paper focuses on the SC at MGS and LGS buildings where demand charges apply. Demand charge is the cost associated with the maximum power the smart meter measures in a billing period under one utility account. Table I shows the demand charge rates from BC Hydro for MGS and LGS [3]. Demand charges are more critical than energy charges for MGS and LGS sites due to 1) electricity resale is prohibited in many jurisdictions 2) where electricity resale is allowed, energy charges can be recovered from drivers, that is, drivers pay by $/kWh but hosts still need to pay for demand charges 3) demand charges may exceed energy charges. For example, for the busiest L2 station in B.C. (Table 4 in [4]), the average monthly energy cost for the host is C$388, whereas the demand cost could be C$474.

TABLE I
BC HYDRO DEMAND CHARGE RATES

Tier	Rate [C$]
First 35 kW	0.00
Next 115 kW	5.72
Remaining kW	10.97

Demand charges from EV charging can be controlled on EVSEs integrable to the distribution or building grid. Utility-integrated EVSEs may be leveraged by the AMI mesh network and Business-to-Business (B2B) models. Compatible EVSEs can also be integrated into BEMS as controllable loads. BEMS manages EV charging on behalf of building manager or as facilitator for utility's DR. Fig. 1 shows the general architecture in EV charging control. For the purpose of demand charge reduction, the BEMS pathway provides direct access to real-time building load and aligning SC with building's benefit.

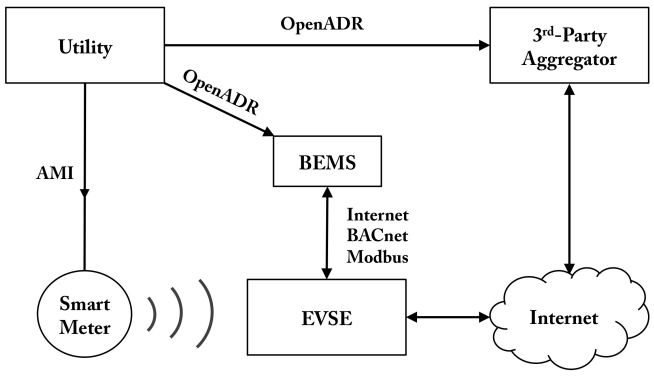

Fig. 1. EV charging control pathways

Most literature on SC deal with long plug-in durations and probabilistic data to infer EV charging demand and plug-in times in the residential context [5]–[11]. In particular, residential SC has been extensively studied because it typically addresses substation demand peak and the fact that more than 80% EV charging occur at home [12], [13]. As charging infrastructure grows, range anxiety from drivers will ease, and non-residential charging activities will keep growing [4]. From a practical point of view, demand charge reduction requires real-time track of demand (at least synchronized with smart meters) with prompt and accurate control that cannot fully rely on probabilistic data. The SC control at non-residential sites also requires granularity to handle more frequent EV mobility and individual charging satisfaction.

In general, unidirectional SC in the literature are designed for 1) minimizing grid impact from various aspects [7], [14], [15], 2) multi-level charging control minimizing charging cost on all stakeholders [5], [16], [17], 3) TOU-based charging for cost minimization [18], 4) integrated charging with renewable generation [19]. Few studies directly deal with demand charges for EVSE hosts. However, some existing approaches are adaptive to non-residential SC.

Chen et al. [15] prove that, in offline cases, valley filling in SC generates the optimal and unique charging profile independent of the power flow optimization from the grid. For online cases, charging deadlines are considered to address the uncertainties in predicting non-EV and EV loads that are used to infer the optimal valley level. Gan et al. [5] propose two SC algorithms-Optimal Decentralized Charging (ODC) and Asynchronous ODC (AODC). Both algorithms are proved to provide the optimal valley filling regardless of EV plug-in time, charging deadline, energy demand, and maximum charging rate. Real-time ODC (RTODC) considers EVs that are currently plugged in but EV uncertainties towards charging deadlines potentially cause charging rebound. Grid-level rebound could be controlled by charging coordination over night [20], whereas building-level SC is not so flexible considering that the average charge events at the top busiest L2 stations are less than 2 hours [4]. Charging can also be controlled based on the prediction of EV availability [11]. However, unlike at substation level, the prediction of EV loads in the C&I context is challenged by EV mobility. Although prediction could be achieved by machine learning and mathematical models [21], [22], more studies are needed for generalization in various host types. Another factor that drives SC is price-based charging in which energy charges are typically considered [18], [22]. Regarding demand charges reduction, rates issued by utilities may not correspond to local demand peaks, thus the impact on EVSE hosts will be sub-optimal or even adverse.

This paper elaborates the valley-filling SC for demand charge reduction at C&I sites where EVSE hosts manage L2 stations for OPEX reduction. We use the term water filling to denote combined valley filling and peak shaving. EVSE hosts may publish power limit on the building grid as the highest water level for demand charges reduction. The paper aims to find SC solutions to handle high EV mobility and the charging rebound problem. The main contributions include:

- Evaluation of real-world SC potential at various non-residential sites

This article has been accepted for publication in a future issue of this journal, but has not been fully edited. Content may change prior to final publication. Citation information: DOI 10.1109/TSG.2016.2647620, IEEE Transactions on Smart Grid

- Real-time SC in non-residential context with tight control flexibilities, adapting to both grid and local DRLC
- Prioritized charging based on arrival and departure times and energy demand to 1) satisfy EV charging requirement, and 2) reduce optimization dimensions
- Balance of demand charge savings and the quality of EV charging service
- SC for C&I sites where demand charges are more critical than energy charges or energy cost can be recovered as station usage fees

Many L2 stations in B.C. are free to customers and employees, so a decrease in OPEX by SC will encourage the growth of public charging infrastructure.

The remaining of the paper is organized as the following: Section II studies real-world EV charging data at different non-residential venues and analyzes EV charging flexibilities. Section III analyzes demand charge saving potential in a deterministic case, and discusses the real-time smart charging algorithm. Section IV presents SC results and evaluates the performance. Section V concludes this paper.

II. EV CHARGING FLEXIBILITY ANALYSIS

This paper uses real-world EVSE data from evCloud[1] to analyze charging flexibility and develop the SC algorithm. We choose data from public L2 stations of different venue types for analysis: large retail, medium retail, workplace/small business and recreation. L2 stations are mainly focused in this paper because of their high volume of usage (compared to DCFCs) and wide availability. L2 stations in B.C. typically allow up to 7.2 kW charging rate.

The L2 charging power follows a nonlinear curve [23], featuring a constant-current (linear) and constant-voltage mode (nonlinear). The original curve in Fig. 2 shows the typical charging profile of Nissan Leaf MY13 [24].

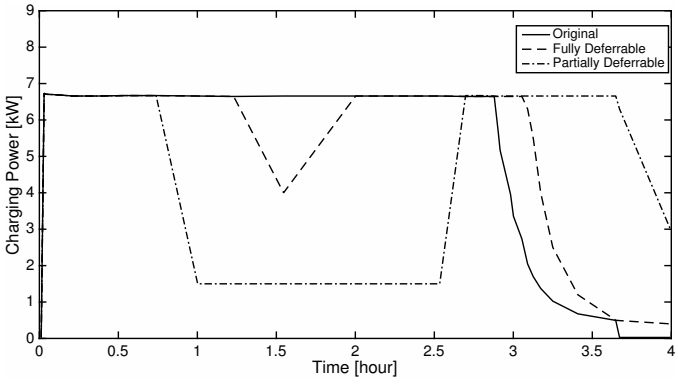

Fig. 2. Nissan Leaf MY13 AC charging profile (adapted from [24]) and illustration of flexible charging

Compared to constant-current charging, charging in constant-voltage mode could be viewed as less efficient charging that can be targeted by load curtailment. SC could defer charging loads in the constant-current mode to the constant-voltage period, potentially increasing charging flexibility at tightly constrained venues.

[1]evCloud: www.fleetcarma.com/evcloud

Definition 1. *Charging sessions with constant-voltage mode longer than Δt are flexible. Otherwise the charging sessions are inflexible.*

In this paper, flexible charging is further categorized as fully and partially deferrable charging (Fig. 2) as (1). For simplicity, both types are referred as deferrable.

$$\text{Fully Deferrable} \Leftrightarrow \int L_{FD}dt = \int L_0 dt, \quad (1a)$$

$$\text{Partially Deferrable} \Leftrightarrow \int L_{PD}dt < \int L_0 dt. \quad (1b)$$

A. Sample EVSE Site

EV charging at large retails features shorter charging duration and higher EV mobility. The studied large retail location is equipped with dual-port EVSEs with dedicated 30A circuit for each port at 240V. More than 80% of the charging sessions are shorter than 3 hours. We categorize EVs into two groups based on typical charging rates, 3.6 and 6.6 kW. Each EV is assumed being charged at 90% efficiency during the constant-current mode. We use the typical charging rates and charging efficiency to infer the time needed for each EV to complete constant-current charging. The rest of the plug-in time is considered as flexible times that the constant-current charging can be deferred to. Completing the constant-current charging session could at least charge EVs to a relatively high SOC (e.g. 86% for LEAF MY13 [24]). In practice, users may choose to opt out if they prefer top-ups.

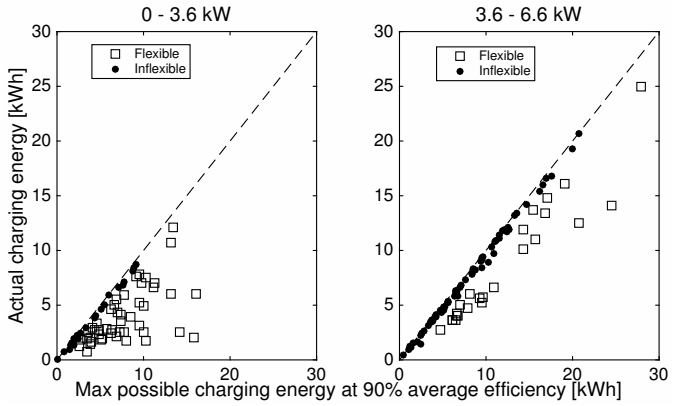

Fig. 3. EV charging flexibility analysis on real-world data

Fig. 3 illustrates the potential charging flexibility from realistic charging data in a week. The x-axes represent the maximum possible charging energy if charging is sustained in constant-current mode during the full charging session. The y-axes show the corresponding actual amount of energy dispensed. Most the points far away from the 45° line correspond to top-up charging in constant-voltage mode for typical EVs. A total of 164 charge events occur during this selected week, 71 (43%) of which are flexible according to Definition 1 with $\Delta t = 15$ min. Note that some squares correspond to old PHEVs, but based on their market share in B.C. [1], PHEVs with low charging rates are not considered in this paper.

This article has been accepted for publication in a future issue of this journal, but has not been fully edited. Content may change prior to final publication. Citation information: DOI 10.1109/TSG.2016.2647620, IEEE Transactions on Smart Grid

B. Charging Flexibility Summary

Table II summarizes charging flexibility analysis for all selected venues, assuming $\Delta t = 15min$. Workplace and recreation venues see the most charging flexibilities due to longer plug-in durations.

TABLE II
EV CHARGING FLEXIBILITY SUMMARY BASED ON REAL-WORLD DATA

Venue type	Flexible charge sessions[i]	Flexible duration[ii]	Average deferrable energy[iii]	Average charging power[iv]
Retail large	43%	58 min	2.8 kWh	3.8 kW
Retail small	46%	53 min	2.4 kWh	3.7 kW
Recreation	58%	58 min	3.7 kWh	4.2 kW
Workplace	61%	90 min	8.1 kWh	3.4 kW

i Derived from Fig. 3.
ii Average duration in constant-voltage charging mode and/or full charge. Deferred energy (column 4) from constant-current charging mode is potentially recoverable in this time period.
iii For each EV, this refers to the maximum amount of energy in constant-current period (if exists) that can be deferred to constant-voltage period if the original energy dispensed in constant-voltage period is deducted. This column represents the maximum energy could be curtailed without severely depreciating charging.
iv Average charging power per EV, or the potential demand peak reduction per EV.

In the lack of granular charging profiles and SOC data, Flexible Duration in Table II is estimated as (2). The Average Deferrable Energy in Table II is simplified as (3).

$$T_F = t_u - (t_p + \frac{E_d}{p_c \cdot \eta}). \tag{2}$$

$$\widetilde{E} = \min(T_F \cdot p_c \cdot \eta, \quad E_d). \tag{3}$$

III. THEORETICAL ANALYSIS

A. Offline Charging Control

This section discusses an offline scenario with water-filling charging algorithm to demonstrate the maximum potential in demand charge reduction from the aggregate level. The a priori inputs used in this section are:

- Real-world start and end times of EV charging sessions
- Energy dispensed in each session

The water-filling algorithm aims to achieve an aggregate load profile (base + EV load) with minimum possible variance. The water-filling concept in this section is different from [5] and [15] in tighter EV constraints. Refs. [5] and [15] prove that the water-filling is optimal and equivalent to minimizing the load variance, or the ℓ^2 norm of the charging profile, Y. The offline results are compared with the online water-filling algorithm discussed in Section IV.

The offline water-filling problem on the aggregate level could be defined as:

$$min: \qquad ||Y||_2, \tag{4a}$$

$$Y = (y_1, y_2, ..., y_t, ...y_T) \in \mathbb{R}^T, \tag{4b}$$

$$y_t = x_b + X_{EV}, \tag{4c}$$

$$s.t.: \qquad 0 \le X_{EV} \le \eta \cdot \sum_{i=1}^{N_{EV}} (p_c \cdot a), \forall t \in \mathbb{R}^T, \tag{5a}$$

$$\Delta t \sum_{t=1}^{t_u} X_{EV} \ge \sum_{i=1}^{N_\nu} E_d, \forall t_u \in \mathbb{R}^{N_\nu}, \tag{5b}$$

$$\Delta t \sum_{t=1}^{T} X_{EV} = \sum_{i=1}^{N_{EV}} E_d. \tag{5c}$$

Eq. (5a) describe the bounds of the solving variables, X_{EV}, from the aggregate level. Eq. (5b) denotes $(N_{EV} - 1)$ constraints for the aggregate charging energy at each t_u ($N_\nu < N_{EV}$). At each t_u, the total energy dispensed needs to be no smaller than the total energy demand from all EVs that have finished charging. Eq. (5c) defines the equality constraint for the total energy dispensed to all the EVs when the last EV leaves.

Definition 2. *The water filling solution from the aggregate level (AWF) is feasible and optimal (defined as Type-0 optimal) if each EV is charged exactly by E_d by deadline and the overall water level is at the lowest possible value.*

Definition 3. *For a given aggregate EV charging profile, the AWF solution is reasonably feasible and optimal (Type-S optimal) if it is never less optimal than the Type-0 solution.*

Lemma 1. *For a given aggregate EV charging profile, the AWF solution in the region defined by (5a-5c) is Type-S optimal.*

Proof. Assume

$$\sum_{t=t_p}^{t_u} x = E_d + E_\delta, \forall i \in \mathbb{Z}^{N_{EV}},$$

where x denotes the time-based charging profile of the $i'th$ EV, and E_δ denotes the error in the total charged energy of the $i'th$ EV by t_u.

The Type-0 solution resides in the following feasible region:

$$R_0 : E_\delta = 0, \forall i \in \mathbb{Z}^{N_{EV}}.$$

At $t = T$,

$$\Delta t \sum_{t=1}^{T} X_{EV} = \sum_{i=1}^{N_{EV}} (E_d + E_\delta),$$

therefore $E_\delta = 0$ infers (5c), and:

$$R_0 \subseteq R_1,$$

where R_1 is the feasible region defined by (5c).

Constraint (5b) is equivalent to:

$$\Delta t \sum_{t=1}^{t_u} X_{EV} = \sum_{k=1}^{N_\nu} (E_d + E_\delta) + \sum_{j=1}^{N_r} E_g,$$

$$\sum_{k=1}^{N_\nu} (E_d + E_\delta) + \sum_{j=1}^{N_r} E_g \ge \sum_{k=1}^{N_\nu} E_d,$$

This article has been accepted for publication in a future issue of this journal, but has not been fully edited. Content may change prior to final publication. Citation information: DOI 10.1109/TSG.2016.2647620, IEEE Transactions on Smart Grid

where N_r denotes the number of EVs that are still being charged at t_u, and E_g is the amount of energy the $j'th$ EV in $\mathbb{Z}^{N_r}$ has been charged. $E_d \geq 0$ and $E_g \geq 0$.

When $E_\delta = 0$, $R_0 \subseteq R_2$, and therefore

$$R_0 \subseteq (R_1 \cap R_2),$$

where R_2 is the feasible region defined by (5b).

For random aggregate charging profiles, each optimal water level can be solved in each of the following problem:

$$H_i = F(\{S_i\}),$$

where H_i is a water-filling problem dealing with one type of aggregate charging profile in the scenario set $\{S_i\}$. Within each $\{S_i\}$, the aggregate profile is the same but the EV arrival and departure times vary.

For every $\{S_i\}$, there exists a special case, S_i^*, when:

$$\begin{aligned} t_u^{(k)} &> t_u^{(k-1)}, \quad \text{and,} \\ t_p^{(k)} &> t_p^{(k-1)}, \quad \forall k \in \mathbb{Z}^{N_{EV}}. \end{aligned}$$

In S_i^*, it can be proved that:

$$R_0 = (R_1 \cap R_2).$$

Therefore, the equality in $R_0 \subseteq (R_1 \cap R_2)$ is valid, and the solution in (5a-5c) is feasible and optimal in at least one case while satisfying R_0. In other words, the solution from (5a-5c) is Type-S optimal.

□

Lemma 1 indicates that under one aggregate charging profile, (4a-5c) solve for the most optimal water level that satisfies all charging demands. Depending on the actual EV availability, the solution from (4a-5c) may not always be feasible. However, for random cases, (4a-5c) only cause 3% error in the optimal water level for retail venues (see Appendix).

B. Real-Time Charging Control

1) Overview: This section expands the water-filling to the real-time context. The real-time water-filling algorithm is developed in a decentralized context at the building level. The idea is to implement the water-filling scheme on currently plugged-in EVs with the provision of future high demand. The overall solution resides on the following assumptions:

- The BEMS onsite controls EV charging.
- The BEMS is able to forecast short-term building demand.
- The BEMS has access to individual EV charging data including energy demand, plug-in and unplug time, charging power, and battery SOC.
- The BEMS complies with DR signals from utility.
- EVs do not stay longer than the original leaving time (t_u).

2) Problem Formulation: The proposed approach solves the optimal charging problem in a receding optimization window similar to [25], [26]. At each step, the BEMS receives new status from the building and EVSEs and update charging constraints. The charging objective at the current time instance m is formulated as:

$$min: \quad ||Y||_2, \tag{6a}$$

$$Y = (y_m, ..., y_t, ...y_s) \in \mathbb{R}^{T_s}, \tag{6b}$$

$$y_t = x_b + \sum_{i=1}^{N_t} x^{(i)}, \tag{6c}$$

where s denotes the end of the EV controlling window with length T_s.

The difference from the literature in this paper is that T_s is not the full plug-in duration of an EV, but represents the receding plug-in duration of the EVs with the earliest leaving time in set $\{EV_1\}$, that is:

$$T_s = min(\mathbf{t_u}) - t_m. \tag{7}$$

The span of T_s in the literature is typically chosen as 1) the full-day control window [25] or 2) to the time when the last EV leaves (Eq. (16) in [26]). The full-day span requires a priori knowledge or prediction of all EVs. Option 2) unnecessarily involves more computation in high-mobility scenarios when inputs are frequently updated. In receding horizons, future arrival of EVs will obsolete the previously calculated charging schedule. Thus, receding horizons with longer span contribute less in the dynamic environment.

The definition of T_s in this paper 1) facilitates priority charging for $\{EV_1\}$, and 2) shrinks the receding window. Priority is defined as full charging demand satisfaction for EVs in $\{EV_1\}$. An equality constraint of energy is set specifically for $\{EV_1\}$ in T_s to assign high priority. The optimization of other EVs, $\{EV_{(-1)}\}$, only deals with inequality constraints of energy in T_s, allowing more flexibility to accommodate the immediate deadline of $\{EV_1\}$. At each step in the receding window, $\{EV_1\}$, $\{EV_{(-1)}\}$, and the corresponding constraints are updated. The setup of receding window ensures the optimization horizon does not expand when new EVs arrive, if $\{EV_1\}$ remains the same.

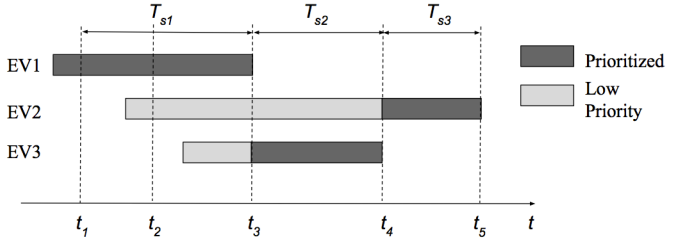

Fig. 4. Receding optimization window with charging priorities

Fig. 4 illustrates the concept of receding optimization window with prioritized charging. In an ideal case when the information of all EVs in the current optimization window is a priori at random t_m, the constraints for $\{EV_1\}$ and $\{EV_{(-1)}\}$ could be expressed as (8-13) and the problem can be solved at $\{EV_1\}$ and $\{EV_{(-1)}\}$ levels.

This article has been accepted for publication in a future issue of this journal, but has not been fully edited. Content may change prior to final publication. Citation information: DOI 10.1109/TSG.2016.2647620, IEEE Transactions on Smart Grid

$$\Delta t \sum_{t_m}^{t_s} x^{(j)} = E_{\epsilon}^{(j)}, \quad \forall j \in \mathbb{Z}^{N_{EV}^*}. \tag{8}$$

$$E_{\epsilon}^{(j)} = E_d^{(j)} - \Delta t \sum_{t=t_p^{(j)}}^{t_m} x^{(j)}. \tag{9}$$

$$E_{(-)} \leq \Delta t \sum_{k=1}^{N_{EV}-N_{EV}^*} \sum_{t_m}^{t_s} x^{(k)} \leq E_{(+)}, \forall k \in \mathbb{Z}^{N_{EV}-N_{EV}^*}. \tag{10}$$

$$E_{(+)} = T_s \sum_{k=1}^{N_{EV}-N_{EV}^*} p_c^{(k)}. \tag{11}$$

$$E_{(-)} = \sum_{k=1}^{N_{EV}-N_{EV}^*} \Big(E_{\epsilon}^{(k)} - (t_u^{(k)} - t_s) * p_c^{(k)} \Big). \tag{12}$$

$$p_{min} \leq x^{(i)} \leq p_c^{(i)}, \quad j \cup k = i. \tag{13}$$

Constraints (8-9) ensure priority charging for all EVs in $\{EV_1\}$. Constraints (10-13) define the bounds for $\{EV_{(-1)}\}$ that accommodate $\{EV_1\}$ priority while ensuring each demand in $\{EV_{(-1)}\}$ be satisfied in the future when the EV moves into $\{EV_1\}$. $E_{(+)}$ and $E_{(-)}$ respectively concern the periods in $[t_m, t_s]$ and $(t_s, t_u]$. A potential problem in constraints (8-13) is the possibility of new demand peak towards t_s, similar to the RTODC (Real-time Optimal Decentralized Charging) results from Figs. 11-12 in [5]. The new peak could be caused by 1) demand rebound from plugged-in EVs when more EVs are grouped into $\{EV_1\}$, and 2) demand from new arriving EVs close to t_s.

The solution to this problem is to reformulate (10-13) to manage charging on individual EVs. Eqs. (14-16) are the new constraints on individual EVs. The upper bound (14) defines the maximum energy can be charged into the $i'th$ EV by t_s. The lower bound (16) is based on the maximum energy can be charged between t_s and $t_u^{(i)}$.

$$E_{(-)}^{(i)} \leq \Delta t \sum_{t_m}^{t_s} x^{(i)} \leq E_{(+)}^{(i)}, \quad \forall i \in \mathbb{Z}^{N_{EV}}, \tag{14}$$

$$E_{(+)}^{(i)} = T_s \cdot p_c^{(i)}. \tag{15}$$

$$E_{(-)}^{(i)} = E_{\epsilon}^{(i)} - (t_u^{(i)} - t_s) \cdot p_c^{(i)}. \tag{16}$$

To further handle potential peaks towards each t_s caused by uncertainties such as the leaving times of plugged-in EVs and number of new arriving EVs, a dynamic LB, p_ζ, for the real-time water-filling problem is defined in (17).

$$p_\zeta = min(p_\lambda, \quad p_\upsilon), \tag{17a}$$

$$\theta = E_\epsilon / E_{max}, \tag{17b}$$

$$E_{max} = (t_u - t_p) \cdot p_\upsilon, \tag{17c}$$

$$p_\lambda = \ell(\theta) = \theta \cdot \bar{p}, \tag{17d}$$

$$\bar{p} = E_d / (t_u - t_p). \tag{17e}$$

p_λ reduces the likelihood of high peak towards each t_s. θ is derived based on Fig. 3. E_d and E_{max} represent the y-axis and x-axis of Fig. 3.

In this paper, p_λ is defined as a linear model of θ. EVs with low flexibility (larger θ) are assigned with higher p_λ. At each time step, θ is updated. For the charging profile of each EV, $\bar{p}$ denotes the optimal water level that also ensures charging demand satisfaction. θ scales $\bar{p}$ down to increase overall charging flexibility. Compared to zero-kW lower bound, p_λ avoids inflexibility and high peak towards t_s by allowing a non-zero minimum charging power throughout the session. Eq. (17) also ensures EVs with high flexibility be utilized for demand shift, and EVs with low flexibility be prioritized for full charge. Fig. 5 illustrates the concept of p_ζ, in which the result from p_ζ (S2) allows higher flexibility towards the end if new EVs arrive.

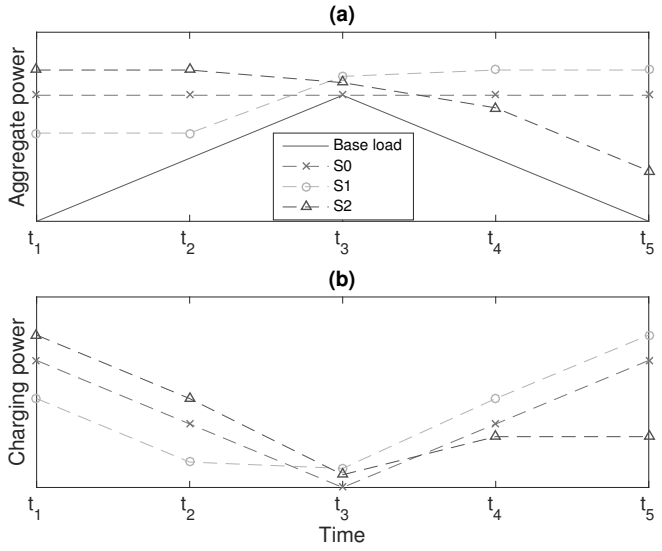

Fig. 5. Concept of dynamic lower bound (S0: perfect water-filling. S1: fixed lower bound at 0 kW. S2: dynamic lower bound)

Eq. (18) defines a new constraint that accommodates local and utility DRLC. Note that high-criticality and aggressive DRLC may cause charging dissatisfaction.

$$\sum_{i=1}^{N_t} (x^{(i)}) + x_b \leq P_\upsilon, \forall t \in [\tau_1, min(\tau_2, t_s)]. \tag{18}$$

In addition, the DRLC will affect the optimization in the succeeding optimization frames by altering the energy constraints in (8-9) and (14)-(16). In particular, (9) for the $j'th$ EV will be transformed to (19):

$$E_\epsilon = E_d^{'} - \Delta t \sum_{t=\tau_2}^{t} x, \quad \forall t \in (\tau_2, t_s], \tag{19a}$$

$$E_d^{'} = min\Big(E_d - \Delta t \sum_{t=t_p}^{\tau_2} x, \quad p_\upsilon (t_s - \tau_2) \Big), \tag{19b}$$

$$E_\epsilon = E_d - \Delta t \Big(\sum_{t=t_p}^{t} x + \sum_{t=\tau_1}^{t} (\widetilde{x} - x) \Big), \forall t \in [\tau_1, \tau_2], \tag{19c}$$

where $\widetilde{x}$ is the calculated power of the $j'th$ EV at $\tau_1 - 1$ for $t \in [\tau_1, \tau_2] \in [t_p, t_u]$ when the DRLC is not anticipated by

This article has been accepted for publication in a future issue of this journal, but has not been fully edited. Content may change prior to final publication. Citation information: DOI 10.1109/TSG.2016.2647620, IEEE Transactions on Smart Grid

the algorithm, and $\tau_1 - 1$ denotes the time instance before the DRLC event starts.

Eq. (19b) compares the original demand after curtailment with the maximum possible energy after τ_2, ensuring that each EV is charged by the maximum amount close to its original demand. During the DRLC event, (19c) relaxes the modified optimization problem in $[\tau_1, \tau_2]$ for general feasibility by assuming the curtailed energy is not deferrable. Algorithm 1 summarizes the real-time water-filling algorithm (RTWF-n1).

Algorithm 1: Real-time water filling with priority charging

Input

- Every month: monthly maximum demand estimation
- Every time step:
  - Building: real-time demand, x_b
  - EV: plug-in times (t_p, t_u), SOC, typical charging rate (p_c), energy demand (E_d), number of EVs (N_{EV}, N_t, N_ν), energy charged to each EV ($\Delta t \sum x$), EV groups ($\{EV_1\}, \{EV_{(-1)}\}$), optimization window based on $\{EV_1\}$ (T_s)

Settings and Calculation (at each time step)

- Initial points for optimization: $x_0 = min(p_\lambda, p_\upsilon) \in \mathbb{R}^{N_t \times (t_s - t)}$
- Max/min energy can be charged to the $i'th$ EV: $E_{(+)}$, $E_{(-)}$
- Set up optimization constraints:
  - $\{EV_1\}$: Energy equality constraint from (8)
$$\Delta t \begin{bmatrix} \sum_{t=t_m}^{t_s} x_t^{(1)} \\ \vdots \\ \sum_{t=t_m}^{t_s} x_t^{(N^*_{EV})} \end{bmatrix} = \begin{bmatrix} E_\epsilon^{(1)} \\ \vdots \\ E_\epsilon^{(N^*_{EV})} \end{bmatrix}$$
  - $\{EV_{(-1)}\}$: Energy inequality constraint from (15-18)
$$\mathbf{E}_{(-)} \leq \Delta t \begin{bmatrix} \sum_{t=t_m}^{t_s} x_t^{(1)} \\ \vdots \\ \sum_{t=t_m}^{t_s} x_t^{(N_{EV}-1)} \end{bmatrix} \leq \mathbf{E}_{(+)}$$
- Bounds: update θ and re-evaluate p_ζ based on x in $[t_p, t_m]$
- Adjust for DRLC:
  - Save $\widetilde{x} \in \mathbb{R}^{N_t \times (\tau_2 - \tau_1)}$ at $t = \tau_1 - 1$
  - Update E_ϵ in (19)

Output (at each time step)

- $x_t^{(i)} \in \mathbb{R}^{N_t \times T_s}, t \in T_s, i \in N_t$
- $\mathbf{x_{t=t_m}} \in \mathbb{R}^{N_t}$ as the final solution at t_m

IV. NUMERICAL RESULTS

A. Offline Results

Fig. 6 shows the offline water-filling results for four types of venues on a single day, considering 30% EV demand penetration level. Each subplot compares the total demand of the building with and without the water-filling. The base load denotes the building's demand without EV.

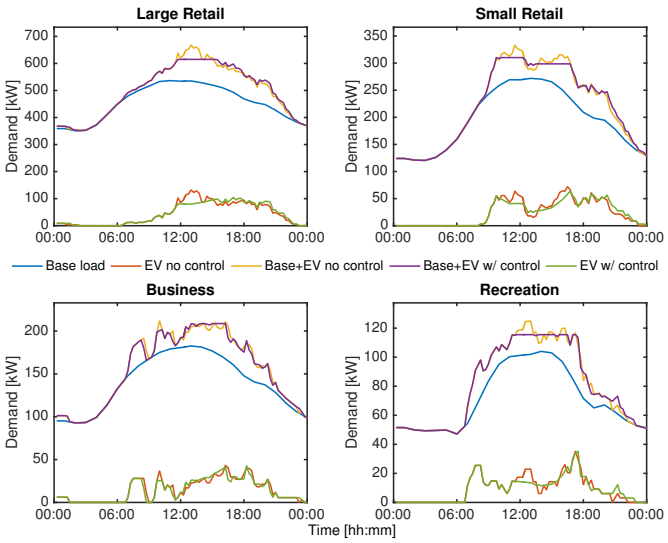

Fig. 6. Offline water-filling results

Table III shows the theoretical savings in demand charges if the peaks in Fig. 6 are the highest in the month. The peak reduction percentages are based on the EV peaks before the water-filling. Generally, venues with higher charging flexibility tend to see more savings in demand charges by EVs.

TABLE III
ESTIMATED MONTHLY DEMAND CHARGE SAVINGS

	Large Retail	Small Retail	Business	Recreation
Peak reduction (kW)	52.33 (40%)	22.83 (37%)	2.95 (10%)	9.39 (45%)
Savings (C$)	574.02	250.39	32.33	53.72

B. Real-Time Results - No DRLC

The RTWF-n1 algorithm is tested on the large retail venue. Real-world charging data from multiple days are lumped into one day to form large penetration levels. The RTWF-n1 performs optimization at 15-minute frequency. Building load profile is obtained from the LGS sector in [27]. Two scenarios are tested-1) RTWF without DRLC, and 2) with DRLC. Scenario 1) maintains that all EVs are charged to the user set points, and Scenario 2) is tested to balance peak reduction and EV charging satisfaction. The RTWF-n1 is carried out in MATLAB R2015b on a computer with 2.26 GHz Intel Core 2 Duo and 8 GB RAM. For 164 EVs (30% penetration), the optimization at each control step takes 0.2-0.3s on average thanks to the linear formulation of the RTWF-n1.

Fig. 7 compares the aggregate EV charging profile under RTWF-n1 with the profile under no control for 30% EV penetration level. The result satisfies (1a). Fig. 7 shows that close to 25 kW peak demand can be avoided. That is, almost 50% of the theoretical maximum, 52 kW, from Table III. Assuming EVs' unplug time uncertainty has a mean of 15 minutes and variance of 10 minutes, about 20 kW peak can still be reduced in this scenario.

This article has been accepted for publication in a future issue of this journal, but has not been fully edited. Content may change prior to final publication. Citation information: DOI 10.1109/TSG.2016.2647620, IEEE Transactions on Smart Grid

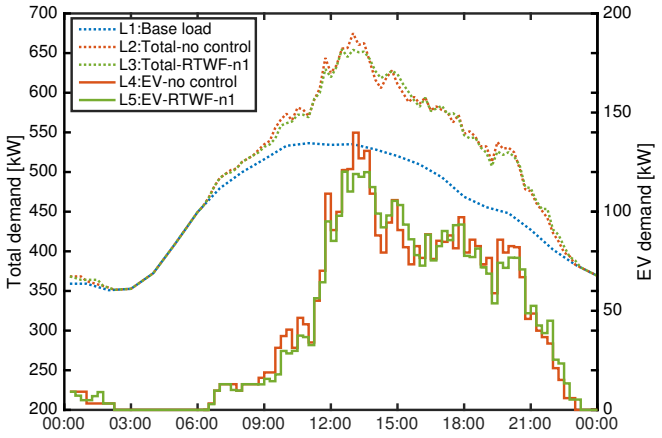

Fig. 7. Scenario 1) result - full charging accommodation

C. Real-Time Results - With DRLC

Both the building-level curtailment and utility DRLC are simulated. Fig. 8 illustrates the results. The BEMS is assumed to publish a 630 kW limit throughout the day, and the utility negotiates a 520 kW limit on the building during the evening peak hours. Charging sessions outside the control windows are controlled without prior knowledge of the DRLC events.

The BEMS local curtailment occurs from 12:30 to 14:00, reducing 45 kW peak demand (86% of the theoretical maximum) on the cost of 0.7 kWh deduction per affected EV. For a LEAF MY13 with 24-kWh battery, that is about 3% SOC less. As a comparison, in the case when RTWF-n1 is not applied and the BEMS publishes the 630 kW limit regardless, curtailed EVs will have 2.3 kWh less, or 10% SOC less for LEAF MY13 and 14% for Volt MY13 (16.5 kWh). Therefore, another benefit of the RTWF-n1 is to balance the impact on both EVSE hosts and EV drivers.

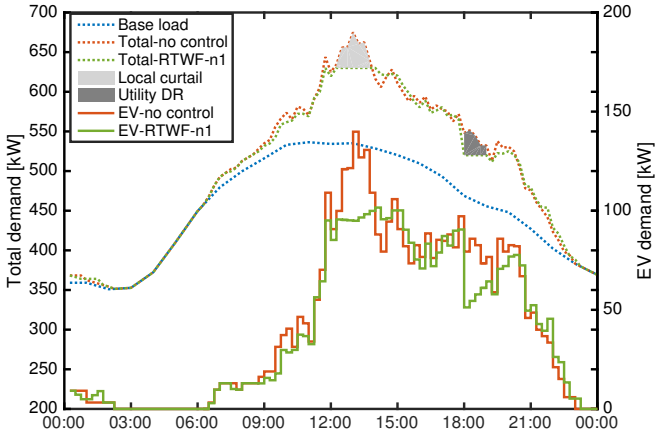

Fig. 8. Scenario 2) result - local and utility DRLC

Upon two DRLC events, around 2.6 kWh energy is deducted from each curtailed EV. Nevertheless, 94% of the daily charging energy demand could still be satisfied while the building could potentially reduce $500 demand charges per month. Both DRLC signals need to coordinate with each other to reduce the impact on EV drivers. Recall that this paper assumes each EV stays no longer than its original deadline, t_u. The RTWF-n1 under DRLC charges fully deferrable EVs to full demand, and partially deferrable EVs by the most possible amount of energy before deadline (19).

Fig. 9 shows how individual EVs respond to the local DRLC signal between 12:30 and 14:00. EV 19 and 24 pause charging temporarily to give priorities to EV 30, 33-35 and 38 which need to meet charging deadlines. EVs undergo the whole DRLC event charge at slower rates and recover back up after the event. Each EV is bounded by its own highest charging rate (3.6 or 6.6 kW times efficiency).

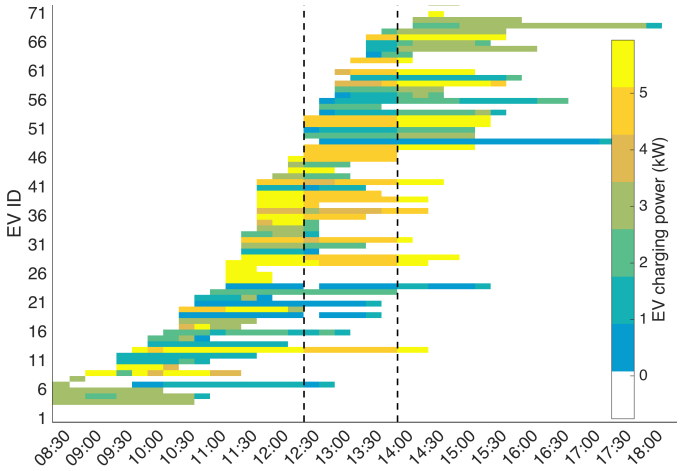

Fig. 9. Estimated EV charging profile under DRLC

D. Real-Time Results - Other Venues

Compared with the large retail venue, EVs at locations with longer plug-in duration will be more flexible and the benefit of RTWF-n1 will be more substantial. Based on the data that we cannot disclose, the RTWF-n1 without DRLC at typical C&I workplace can avoid 50 kW peak demand for 30% EV penetration (or 60 EVs in this case), which is equivalent to $6000 annual demand charge savings.

E. Real-Time Results - Sensitivity

This section examines the performance of the RTWF-n1 in various scales, and compares the results with different algorithm settings. Fig. 10 shows that the RTWF-n1 without DRLC generally reduces half of the possible reduction amount. The RTWF-n1 with dynamic LB and variants outperforms that with fixed LB as more EVs plug in. In the refined-LB case, dynamic LBs are applied only during high-volume EV inrush. More peak reduction can be achieved as a result. The DRLC maintains each affected EV is curtailed by less than one kWh.

For large scales with more EVs and less flexibility, inflexible EVs are excluded from the RTWF-n1 problem. The overall demand still counts the inflexible EVs. Large scales do not affect the RTWF-n1 structure. However, receding windows will be updated more frequently.

Fig. 11 compares the impact of DRLC on EV charging demand. The same DRLC signals are applied to both methods.

This article has been accepted for publication in a future issue of this journal, but has not been fully edited. Content may change prior to final publication. Citation information: DOI 10.1109/TSG.2016.2647620, IEEE Transactions on Smart Grid

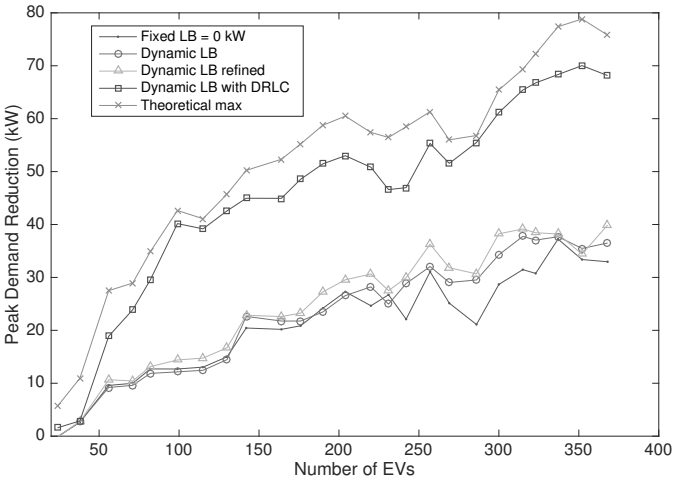

Fig. 10. Peak reduction sensitivity (large retail)

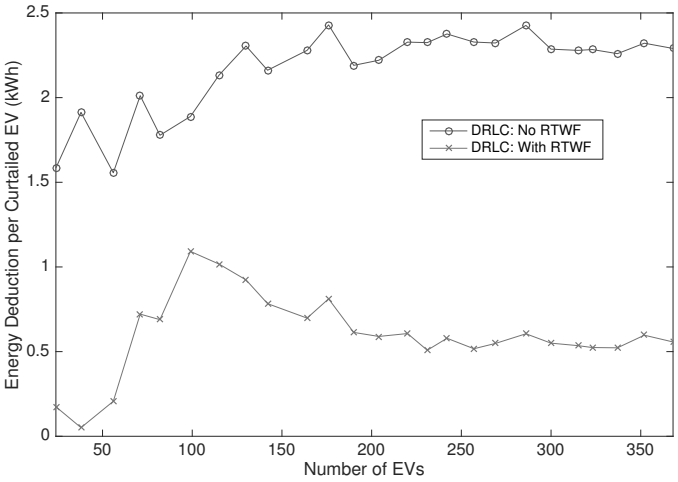

Fig. 11. Comparison of EV charging demand deduction under DRLC

The DRLC combined with RTWF-n1 shows less impact on EV drivers compared to the fixed-power-limit case.

Fig. 12a shows the average dimension reduction of RTWF-n1 under various EV penetration levels. The Principle Component Analysis (PCA) in Fig. 12b shows that the dimension reduction percentage, $\mathcal{O}$, is inversely affected by N_m and ψ_m. This is because the priority charging limits the optimization problem in each receding window to expand only on the direction of N_m, not on the time horizon. When the current EVs in $\{EV_1\}$ remain plugged in, new arriving EVs are only possible to shrink the length of the receding window if they leave earlier than $\{EV_1\}$. The receding window remains the same if the new arriving EVs leave later than the current $\{EV_1\}$. When EV charging deadlines are close to each other at large scales, $\mathcal{O}$ saturates around 40%.

F. Financial Analysis

This section studies the energy cost on EVSE hosts and drivers under the RTWF-n1 in a two-tier TOU context. The water filling of demand inherently reduces energy cost if the base load profile follows the TOU profile. We consider various on-peak windows with different start and end times, and generated Fig. 13 for the average energy savings per EV[1]. The total savings for the host are summarized and compared in Table IV.

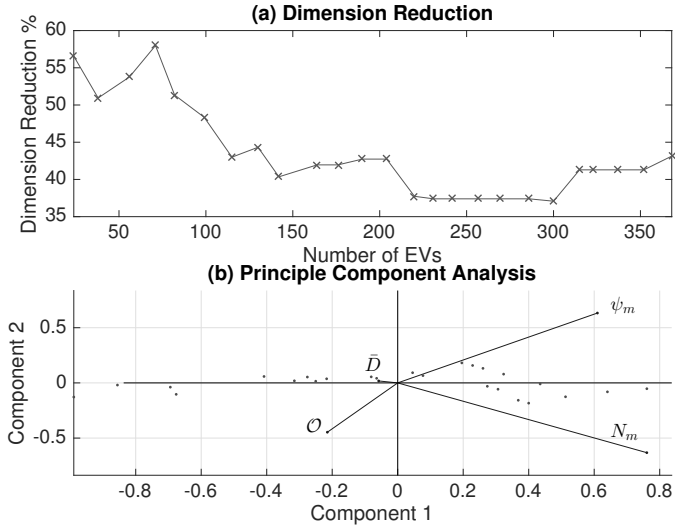

Fig. 12. Dimension reduction in RTWF-n1 ($\mathcal{O}$: dimension reduction, $\bar{D}$: average plug-in duration, N_m: max number of EVs charging at the same time, ψ_m: max number of EVs that arrive/leave at the same time)

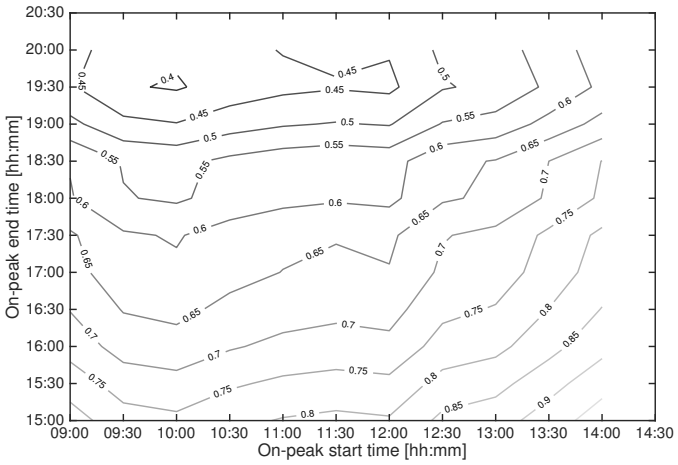

Fig. 13. Average energy cost reduction ($) by RTWF-n1 no DRLC for each EV in a day. Off-peak rate: $0.0536/kWh; on-peak rate: $0.1072/kWh

For locations where electricity resale is prohibited, EVSE hosts have limited options for reducing energy cost. For other locations where energy cost can be recovered by $/kWh or parking, EVSE hosts will mainly need to concern demand charges. However, EVSE hosts may need to consider low energy rates for drivers so that public charging is not discouraged.

In case of free charging, moderate DRLC that may reduce small amount of charging energy on particular EVs is more likely acceptable for general drivers. In case charging

[1]Consider $0.0536/kWh for Part-1 energy charge for LGS, assuming the overall energy is around baseline. (https://www.bchydro.com/accounts-billing/rates-energy-use/electricity-rates/business-rates.html)

This article has been accepted for publication in a future issue of this journal, but has not been fully edited. Content may change prior to final publication. Citation information: DOI 10.1109/TSG.2016.2647620, IEEE Transactions on Smart Grid

TABLE IV
MONTHLY SAVINGS COMPARISON FOR 30% EV PENETRATION AT LARGE RETAIL

RTWF-n1	Energy savings[i]	Demand savings	Total savings
No DRLC	C$102	C$263	C$365
Local DRLC	C$173	C$494	C$667
Two DRLC	C$251	C$494	C$745[ii]

i Assuming curtailed energy as savings for the host
ii Omitting incentives from utility for DR support

is not free, because the demand charges savings are more compelling, EVSE hosts will have flexible options for compensating drivers who opt in DRLC (e.g. discount offer).

V. Conclusion

This paper introduces a demand-charge-reducing approach that combines water filling and active DRLC. Real-world EV charging data are used to study the potential in demand charge reduction at non-residential sites. The proposed real-time water filling with priority charging (RTWF-n1) shows that demand charge reduction can reach more than 80% of the theoretical maximum when combined with DRLC. For 30% EV penetration, the studied large retail venue is able to save C$6000 in demand charge per year. The impact of DRLC on EV charging demand is reduced by more than 70% when the RTWF-n1 is applied.

In the future if station hosts install battery systems to further reduce demand charges, the RTWF-n1 is able to help lower the required battery power capacity, thus reducing more demand charges with less capital cost.

Appendix
Error Analysis in Offline Water Filling

Eqs. (4a-5c) may generate infeasible water levels that cannot satisfy R_0 in Lemma 1 when more than three EVs are being charged at the same time, and

$$t_p^{(i)} = min(\mathbf{t_p}), \quad \text{and,} \tag{20a}$$
$$t_u^{(i)} = max(\mathbf{t_u}), \quad \forall i \in \mathbb{Z}^{N_t}. \tag{20b}$$

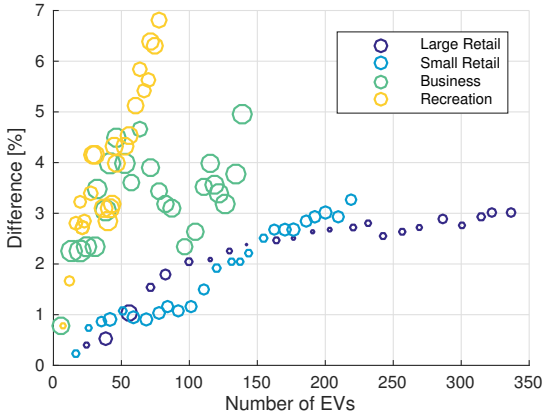

Fig. 14. Type-S (4a-5c) vs Type-0 optimum (21): peak difference in % (circle radii represent average plug-in duration)

To study the infeasibility in (4a-5c) and to avoid optimization in non-deterministic polynomial time (NP) on the aggregate level, we re-solve the offline problem on individual EV level. The new optimization is formulated as a least-square (lsq) problem:

$$min: \quad F = ||\mathbf{C}\mathbf{x}_\ell + \mathbf{X_b}||_2, \tag{21a}$$
$$\mathbf{C} = \begin{bmatrix} \mathbf{U} & \mathbf{0} & \dots & \mathbf{0} \\ \mathbf{0} & \mathbf{U} & \mathbf{0} & \vdots \\ \vdots & \vdots & \ddots & \vdots \\ \mathbf{0} & \mathbf{0} & \mathbf{0} & \mathbf{U} \end{bmatrix}, \tag{21b}$$
$$\mathbf{U} = [\mathbf{1}] \in \mathbb{Z}^{1\times N_{EV}}, \tag{21c}$$
$$\mathbf{x}_\ell = \begin{bmatrix} \mathbf{x^{t=1}} & \mathbf{x^{t=2}} & \dots & \mathbf{x^{t=96}} \end{bmatrix}^T, \tag{21d}$$
$$\mathbf{x^{t=i}} = \begin{bmatrix} x^{(1)} & x^{(2)} & \dots & x^{(N_{EV})} \end{bmatrix}^T, \tag{21e}$$
$$s.t.: \quad \mathbf{A_{eq}}\mathbf{x}_\ell = \mathbf{E_d}, \tag{21f}$$
$$\mathbf{A_{eq}} = \begin{bmatrix} \mathbf{a_1^{t=1}} & \mathbf{a_1^{t=2}} & \dots & \mathbf{a_1^{t=96}} \\ \mathbf{a_2^{t=1}} & \mathbf{a_2^{t=2}} & \dots & \mathbf{a_2^{t=96}} \\ \vdots & \vdots & \vdots & \vdots \\ \mathbf{a_{N_{EV}}^{t=1}} & \mathbf{a_{N_{EV}}^{t=2}} & \dots & \mathbf{a_{N_{EV}}^{t=96}} \end{bmatrix}, \tag{21g}$$
$$0 \le \mathbf{x}_\ell \le \mathbf{p_c}, \tag{21h}$$
$$\mathbf{p_c} = \begin{bmatrix} \mathbf{p_c^{t=1}} & \mathbf{p_c^{t=2}} & \dots & \mathbf{p_c^{t=96}} \end{bmatrix}^T, \tag{21i}$$
$$\mathbf{p_c^{t=i}} = \begin{bmatrix} p_c^{(1)} & p_c^{(2)} & \dots & p_c^{(N_{EV})} \end{bmatrix}^T. \tag{21j}$$

The lsq problem guarantees feasible solutions. However, (21) requires huge memory to solve at large scales. For example, for 300 EVs at $\Delta t = 15min$, (21) needs to solve for 28,800 variables, requiring more than 8 Gb of memory.

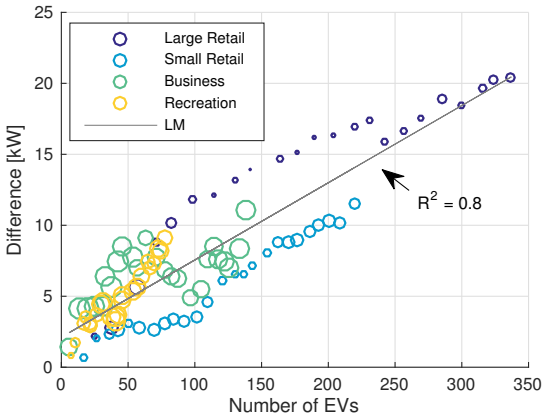

Fig. 15. Type-S (4a-5c) vs Type-0 optimum (21): peak difference in kW

Fig. 14 compares the peak reduction performance between (4a-5c) and (21):

- For large and small retails with frequent EV mobility, the Type-0 optimum from (21) is 3% lower than the Type-S optimum from (4a-5c);
- Error in Type-S optimum is higher at the venues with longer plug-in duration.

With available data, a generic linear model (LM) is approximated in Fig. 15 for all types of venues:

$$P_\epsilon = 0.0544 N_{EV} + 2.116, \tag{22}$$

This article has been accepted for publication in a future issue of this journal, but has not been fully edited. Content may change prior to final publication. Citation information: DOI 10.1109/TSG.2016.2647620, IEEE Transactions on Smart Grid

where P_ϵ denotes the error in the maximum peak shaving potential in (4a-5c).

With the LM and the Type-S solution, the peak shaving potential on daily basis can be efficiently estimated given the historical charging data.

ACKNOWLEDGMENT

The authors would like to thank Powertech Labs for providing the real-world charging data. The evCloud is funded through the B.C. Electric Vehicle Smart Infrastructure Project led by Natural Resources Canada and BC Hydro.

REFERENCES

[1] M. Stevens, "Electric vehicle sales in canada: 2015 final numbers," http://www.fleetcarma.com/ev-sales-canada-2015/, 2016, accessed: 01-May-2016.

[2] "2015 ev charging station infrastructure highlights," https://chargehub.com/blog/en/2015-ev-charging-infrastructure-highlights-2/, 2016, accessed: 01-May-2016.

[3] "General service business rates," https://www.bchydro.com/accounts-billing/rates-energy-use/electricity-rates/business-rates.html#mgs, 2016, accessed: 07-May-2016.

[4] Powertech Labs, "evcloud summary report: B.c. public charging station usage - june 2015 to november 2015," Powertech Labs, Tech. Rep., 10 2016, available: http://www.powertechlabs.com/temp/201610366696/EV_Cloud_Summary_Report.pdf.

[5] L. Gan, U. Topcu, and S. H. Low, "Optimal decentralized protocol for electric vehicle charging," *IEEE Transactions on Power Systems*, vol. 28, no. 2, pp. 940–951, 2013.

[6] Z. Tan, P. Yang, and A. Nehorai, "An optimal and distributed demand response strategy with electric vehicles in the smart grid," *IEEE Transactions on Smart Grid*, vol. 5, no. 2, pp. 861–869, 2014.

[7] L. Hua, J. Wang, and C. Zhou, "Adaptive electric vehicle charging coordination on distribution network," *IEEE Transactions on Smart Grid*, vol. 5, no. 6, pp. 2666–2675, 2014.

[8] Z. Yu, Y. Xu, and L. Tong, "Large scale charging of electric vehicles: A multi-armed bandit approach," in *2015 53rd Annual Allerton Conference on Communication, Control, and Computing (Allerton)*. IEEE, 2015, pp. 389–395.

[9] K. Zhou and L. Cai, "Randomized phev charging under distribution grid constraints," *IEEE Transactions on Smart Grid*, vol. 5, no. 2, pp. 879–887, 2014.

[10] K. Sun, M. R. Sarker, and M. A. Ortega-Vazquez, "Statistical characterization of electric vehicle charging in different locations of the grid," in *2015 IEEE Power & Energy Society General Meeting*. IEEE, 2015, pp. 1–5.

[11] M. F. Shaaban, M. Ismail, E. F. El-Saadany, and W. Zhuang, "Real-time pev charging/discharging coordination in smart distribution systems," *IEEE Transactions on Smart Grid*, vol. 5, no. 4, pp. 1797–1807, 2014.

[12] K. Zhang, L. Xu, M. Ouyang, H. Wang, L. Lu, J. Li, and Z. Li, "Optimal decentralized valley-filling charging strategy for electric vehicles," *Energy Conversion and Management*, vol. 78, pp. 537–550, 2014.

[13] J. Francfort, B. Bennett, R. Carlson, T. Garretson, L. Gourley, D. Karner, M. Kirkpatrick, P. McGuire, D. Scoffield, M. Shirk, S. Salisbury, S. Schey, J. Smart, S. White, and J. Wishart, "Plug-in electric vehicle and infrastructure analysis," Idaho National Laboratory, Tech. Rep., 9 2015, available: https://avt.inl.gov/sites/default/files/pdf/arra/ARRAPEVnInfrastructureFinalReportHqltySept2015.pdf.

[14] I. Sharma, C. Canizares, and K. Bhattacharya, "Smart charging of pevs penetrating into residential distribution systems," *IEEE Transactions on Smart Grid*, vol. 5, no. 3, pp. 1196–1209, 2014.

[15] N. Chen, C. W. Tan, and T. Q. Quek, "Electric vehicle charging in smart grid: Optimality and valley-filling algorithms," *IEEE Journal of Selected Topics in Signal Processing*, vol. 8, no. 6, pp. 1073–1083, 2014.

[16] M. R. Sarker, M. A. Ortega-Vazquez, and D. S. Kirschen, "Optimal coordination and scheduling of demand response via monetary incentives," *IEEE Transactions on Smart Grid*, vol. 6, no. 3, pp. 1341–1352, 2015.

[17] E. Veldman and R. A. Verzijlbergh, "Distribution grid impacts of smart electric vehicle charging from different perspectives," *IEEE Transactions on Smart Grid*, vol. 6, no. 1, pp. 333–342, 2015.

[18] N. Korolko and Z. Sahinoglu, "Robust optimization of ev charging schedules in unregulated electricity markets," 2015.

[19] Y. Guo, J. Xiong, S. Xu, and W. Su, "Two-stage economic operation of microgrid-like electric vehicle parking deck," *IEEE Transactions on Smart Grid*, vol. 7, no. 3, pp. 1703–1712, 2016.

[20] W. Qi, Z. Xu, Z.-J. M. Shen, Z. Hu, and Y. Song, "Hierarchical coordinated control of plug-in electric vehicles charging in multifamily dwellings," *IEEE Transactions on Smart Grid*, vol. 5, no. 3, pp. 1465–1474, 2014.

[21] M. Majidpour, C. Qiu, P. Chu, R. Gadh, and H. R. Pota, "Fast prediction for sparse time series: Demand forecast of ev charging stations for cell phone applications," *IEEE Transactions on Industrial Informatics*, vol. 11, no. 1, pp. 242–250, 2015.

[22] C. Le Floch, F. di Meglio, and S. Moura, "Optimal charging of vehicle-to-grid fleets via pde aggregation techniques," in *2015 American Control Conference (ACC)*. IEEE, 2015, pp. 3285–3291.

[23] K. Qian, C. Zhou, M. Allan, and Y. Yuan, "Modeling of load demand due to ev battery charging in distribution systems," *IEEE Transactions on Power Systems*, vol. 26, no. 2, pp. 802–810, 2011.

[24] "2013 nissan leaf battery charge profiles at different temperatures," https://avt.inl.gov/sites/default/files/pdf/fsev/2013NissanLeafElectricChargingReport.pdf, accessed: 04-May-2016.

[25] M. G. Vayá, G. Andersson, and S. Boyd, "Decentralized control of plug-in electric vehicles under driving uncertainty," in *IEEE PES Innovative Smart Grid Technologies, Europe*. IEEE, 2014, pp. 1–6.

[26] Y. Mou, H. Xing, Z. Lin, and M. Fu, "Decentralized optimal demand-side management for phev charging in a smart grid," *IEEE Transactions on Smart Grid*, vol. 6, no. 2, pp. 726–736, 2015.

[27] "2015 static load profiles," https://www.sce.com/wps/portal/home/regulatory/load-profiles/2015staticloadprofiles/, accessed: 04-Feb-2016.

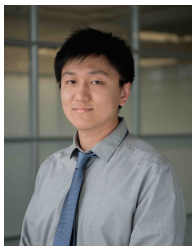

Guanchen Zhang received his B.A.Sc. in Mechatronic Systems Engineering from Simon Fraser University (SFU) in 2013. He is currently pursuing his M.A.Sc. degree at SFU. His research interests include simulation-based optimization, EV smart charging, and residential load disaggregation.

Guanchen Zhang is currently an engineer with Advanced Transportation and Grid Modernization Group at Powertech Labs Inc. His work include usage analysis of public EV charging stations, full-stack web development for EV Demand Response through SMI, and product design and testing for IoTs in smart grid.

Shaoqing Tim Tan received his B.A.Sc. in Mechatronic Systems Engineering from Simon Fraser University in 2014. He had actively participated in multiple projects at the Product Design and Optimization Lab and the Integrated Multi-Transducer Systems Lab at SFU throughout his undergraduate years.

Tim Tan is a senior software developer. In his professional career, he had worked at BlackBerry, Broadcom, Kodak, and Nuvation. He is currently with PowerBeam LLC, changing the world one line of code at a time.

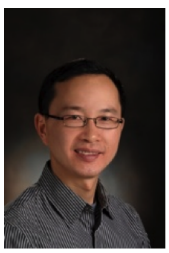

G. Gary Wang is a full professor at Simon Fraser University (SFU) in Vancouver, Canada and an ASME Fellow. He is active in research on design optimization, energy systems, and advanced manufacturing. Dr. Wang is currently serving as an associate editor for Journal of Engineering optimization, geographically covering North America, and associate editor for ASME Transactions, Journal of Mechanical Design.